

---

# Unsteady Numerical Simulation of Cavitation in Axial Turbine

Nabil H. Mostafa and Mohamed Adel<sup>c</sup>

*Mechanical Power Engineering Department, Engineering Faculty  
Zagazig University, Zagazig, 44519, EGYPT*

Received: 06/03/2012 – Revised 16/07/2012 – Accepted 22/10/2012

---

## Abstract

A 3-D numerical study has been carried out in order to study the unsteady, turbulent, void growth and cavitation simulation inside the passage of the axial flow turbine. In this study a 3D Navier-Stokes code was used (CFDRC, 2008) to model the two-phase flow field around a four blades axial turbine. The governing equations are discretized on a structured grid using an upwind difference scheme. The numerical simulation used the standard  $k-\epsilon$  turbulence model to account for the turbulence effect. The numerical simulation of void growth and cavitation in an axial turbine was studied under unsteady calculating. Pressure distribution and vapour volume fraction were completed versus time at different condition. The computational code has been validated by comparing the predicated numerical results with the previous studies. The comparison shows good agreement.

*Keywords: Cavitation; Axial turbine; CFD; Unsteady; Simulation; and void growth.*

---

## 1. Introduction

The cavitation phenomenon is an important cause of wear and damages in hydro-turbines. Cavitation occurs in the flow of water owing to regions of high flow velocity and the local static pressure decreases below the vapour pressure. If at any point liquid flows into a region where the pressure is reduced to vapour pressure, the liquid boils locally and vapour pockets are formed. The vapour bubbles are carried along with the liquid, and when they reach regions of higher pressure, they suddenly collapse. This process is called cavitation. The collapsing action produces high-pressure pulses, often of the order of gigapascals. When such collapse takes place adjacent to solid walls continually and at high frequency, the material in that zone gets damaged. This is called pitting of solid surfaces. Cavitation is also accompanied by noise, vibration, and drop in efficiency.

A limited number of studies tried to simulate the cavitation in axial turbines. An energy model was used to predict the cavitation erosion in centrifugal pumps, but it predicts the hydrodynamic aspect of cavitation this is done by Mostafa, et al. [1]. Nilsson and Davidson [2] developed a parallel multiblock finite volume CFD code for computations of turbulent flow in complex domains for an investigation of the turbulent flow in Kaplan water turbines. This work was focused on tip clearance losses, which reduced the efficiency of a Kaplan water turbine by about 0.5%. Grekula and Bark [3] carried out an experimental study on cavitation processes in a Kaplan model turbine and studied with the aim to identify mechanisms that promote erosive cavitation. The

---

<sup>c</sup> Corresponding Author: Mohamed Adel

Email: [m.adel@zu.edu.eg](mailto:m.adel@zu.edu.eg)

© 2012 All rights reserved. ISSR Journals

PII: S2180-1363(12)43140-X

studies were carried out with high-speed filming, video filming and visual observations with stroboscopic light. A periodic pattern of the cavitating tip vortex was observed. Cavitation at blade root observed. The tip vortex cavitation was characterized by fine scaled cloud cavitation at the points where it approached the blade surface, which indicated an erosion risk. Balint et al [4] carried out a numerical investigation by computing the 3D turbulent single phase flow in the Kaplan turbine runner, the secondary phase for the water (vapour) was activated starting far from the cavitation occurrence conditions. The output pressure in the runner domain was decreased to initiate the cavitating conditions on the runner blades. It was concluded that unsteady effects of the flow have been made mainly by the unsteady detachments of the cavitation at the blade suction side close to the trailing edge. An original method of computing the cavitation inception and of comparing different operating regimes in similar cavitating conditions was presented by plotting the cavitation volume growth. Escalera et al [5] carried out an experimental investigation in order to evaluate the detection of cavitation in actual hydraulic turbines. The methodology was based on the analysis of structural vibrations, acoustic emissions and hydrodynamic pressures measured in the machine. The results obtained for the various types of cavitation found in the selected machines. Mostafa and Boraey [6] made an experimental and numerical study of the two-phase flow field around a four blades axial pump but this study was based on steady conditions as an assumption. Yuliu et al [7] carried out a study of cavitating flow in a Kaplan turbine having numerical simulation with a cavitation model and a mixture two-phase flow model. It was performed to unsteady cavitating turbulent flow within the entire flow passage of a Kaplan turbine in a hydraulic power plant. Based on the calculation results, region and degree of cavitation occurred in the flow passage of the turbine running in a given working conditions. The calculated unsteady cavitation flow results show that the cavitation appears on the suction surface (S.S.); while in the other parts (runner flow passages, spiral casing, guide vanes, draft tube), there is not any cavity observed. Sedlář et al. [8] made Analysis of Cavitation Phenomena in Water and its Application to Prediction of Cavitation Erosion in Hydraulic Machinery. This article also shortly described the experimental research of the cavitating flow aimed at the validation of the erosion potential model, development of the nuclei-content measurement and the validation of the bubble nucleation model. Singh and Nestmann [9] presented an Experimental optimization of a free vortex propeller runner for micro hydro application. This paper presented a wide range of geometrical optimization steps carried out on a propeller runner, whose blades have been designed using the free vortex theory, and operating with a gross head from 1.5 to 2 m and discharge of approximately 75 l/s.

The main objective of this study is to simulate the unsteady 3-D Navier-Stokes equations, behaviour of a cavitating axial turbine with special interest in the cavity geometry, the pressure and void fraction fields. Also, it includes the effects of turbulence and fluid viscosity. The cavity shape will be determined over the blades and the 3-D flow field around the cavitating propeller.

## 2. Theoretical background

The basic approach is to use standard viscous flow (Navier-Stokes) equations with provisions for variable density and a conventional turbulence model, such as K- $\epsilon$  model. A numerical model previously developed by CFDRC [10], [11] to solve (Navier- Stokes) equations this is done by Hinze [12].

The mixture density ( $\rho$ ) is a function of vapour mass fraction ( $f$ ), which is computed by solving a transport equation simultaneously with the mass and momentum conservation equations. The  $\rho$  - $f$  relationship is:

$$\frac{1}{\rho} \equiv \frac{f}{\rho_v} + \frac{1-f}{\rho_l} \quad (1)$$

In two-phase flows, the use of vapour volume fraction ( $\alpha$ ) is also quite common. Therefore, it is deduced from  $f$  as follows:

$$\alpha = f \frac{\rho}{\rho_v} \quad (2)$$

The transport equation for vapour is written as follows:

$$\frac{\partial}{\partial t}(\rho f) + \nabla \cdot (\rho \bar{v} f) = \nabla \cdot (\Gamma \nabla f) + R_e - R_c \quad (3)$$

The expressions of  $R_e$  and  $R_c$  have been derived from the reduced form of the Rayleigh-Plesset equation by Hammit [13] which describes the dynamics of single bubble in an infinite liquid domain. The expressions for  $R_e$  and  $R_c$  are:

$$R_e = C_e \frac{V}{\sigma} \frac{ch}{\rho_l \rho_v} \sqrt{\frac{2 P_{sat} - P}{\rho_l}} (1 - f) \quad (4)$$

$$R_c = C_c \frac{V}{\sigma} \frac{ch}{\rho_l \rho_v} \sqrt{\frac{2 P - P_{sat}}{\rho_l}} f \quad (5)$$

Cavitation normally takes place in the vicinity of low pressure (or locally high velocity) regions, where turbulence effects are quite significant. In particular, turbulent pressure fluctuations have significant effect on cavitating flows. The magnitude of pressure fluctuations is estimated by using the following empirical correlation by Pereira, et al [14]:

$$P'_{turb} = 0.39 \rho k \quad (6)$$

The vapour pressure threshold pressure value is as:

$$p_v = p_{sat} + 0.5 p'_{turb} \quad (7)$$

It is well known that cavitating flows are sensitive to the presence of non-condensable gases. In most liquids, there is a small amount of non-condensable gases present in dissolved and/or mixed state. For example, laboratory water generally has 15 ppm air dissolved in it. In other applications, e.g., marine propellers, etc., this amount may be considerably larger. In this model, the non-condensable gas is included by prescribing an estimated mass fraction at inlet. This value is held constant throughout the calculation domain. However, the corresponding density (and hence volume fraction) varies significantly with local pressure. The perfect gas law is used to account for the expansion (or compressibility) of gas; i.e.

$$\rho_{gas} = \frac{WP}{RT} \quad (8)$$

The calculation of mixture density (equation 1) is modified as:

$$\frac{1}{\rho} = \frac{f_v}{\rho_v} + \frac{f_g}{\rho_g} + \frac{1 - f_v - f_g}{\rho_l} \quad (9)$$

We have the following expression for the volume fractions of vapour ( $\alpha_v$ ) and gas ( $\alpha_g$ ):

$$\alpha_v = f_v \frac{\rho}{\rho_v} \quad (10)$$

$$\alpha_g = f_g \frac{\rho}{\rho_g} \quad (11)$$

$$\alpha_l = 1 - \alpha_v - \alpha_g \quad (12)$$

The combined volume fraction of vapour and gas (i.e.,  $\alpha_v + \alpha_g$ ) is referred to as the Void Fraction ( $\alpha$ ). In practical applications, for qualitative assessment of the extent and location of cavitation, contour maps of void fraction ( $\alpha$ ) are important to determine bubbles location and shape.

### 3. Computational analysis

The numerical simulation was done using a 3-D Navier-Stokes code (CFDRC, 2008) to model the two phase flow field around a 3D rotor in a cavitating axial turbine. This code employs a

homogenous flow approach, also known as Equal-Velocity-Equal-Temperature (EVET) approach (CFDRC, 2008) and Fukaya, et al. [15]. The governing equations are discretized on a structured grid using an upwind difference scheme. The numerical simulation used the standard  $k-\epsilon$  turbulence model to account for the turbulence effect. The cavity shape was determined. Also, various variables were calculated, such as void fraction, mass fraction, pressure and velocity contours. It is clear that the full cavitation model used in this simulation includes a lot of effects which were previously ignored in the previous studies, such as unsteady, fluid viscosity, turbulence and the slip speed factor (ratio between actual and theoretical rotor rotating speed).

#### 4. Boundary conditions

In this case of a four-blade axial flow turbine, sixteen blocks were used to generate the 3D rotor model as shown in figure 1. The structured grid is consisted of about 180,000 nodes. The propeller diameter is 4 in. (101 mm). Reynolds number is about 333,000. The structured grid geometry of the rotor is constructed at three blade angles  $60^\circ$ ,  $70^\circ$  and  $80^\circ$ . In order to simulate the rotation in the structured grid of the rotor, a rotating frame of the grid was assumed around the rotor axis, the slip speed factor of the rotating frame is equal to 0.67. The unsteady time step was  $1.2 \times 10^{-4}$  sec. The computational time was about 20 minutes for one time step. The computer used was Intel Core i5 Processor 2.4 GHz, and 4 GB RAM.

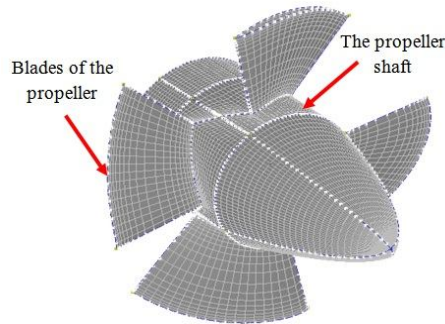
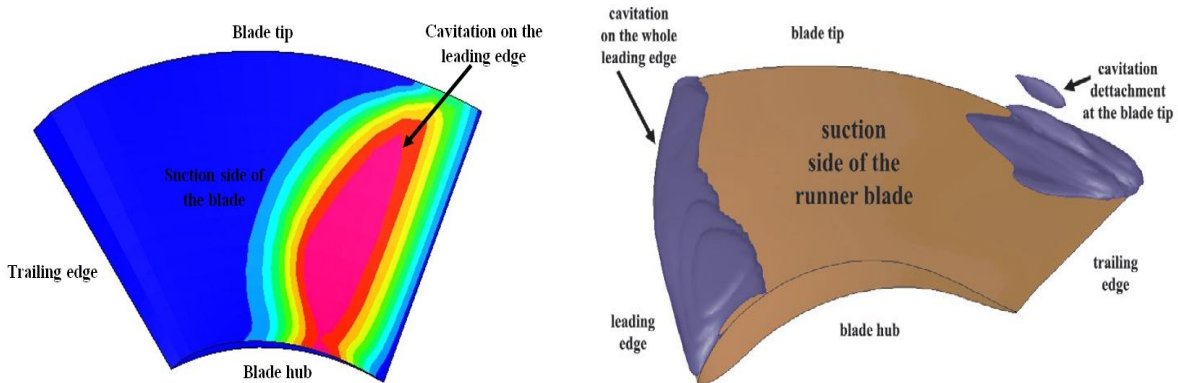


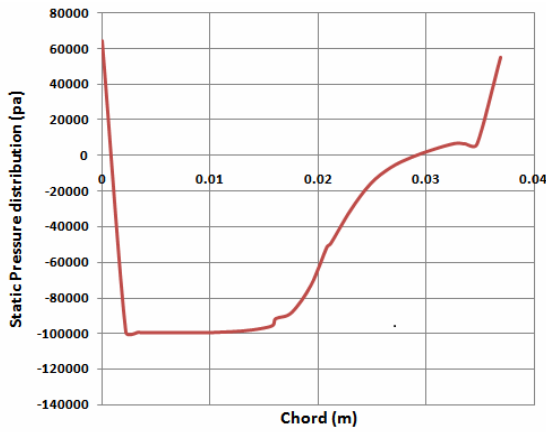
Figure 1. Geometry technique for the axial turbine.

#### 5. Validation results

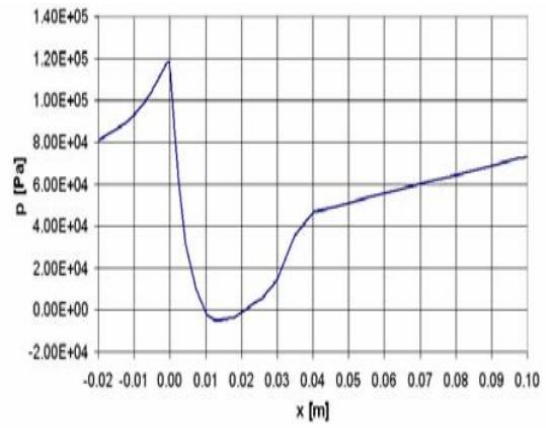
Figure 2 shows a comparison between the present numerical result, which is presented in Figure 2a, and the result of Balint et al. [4], Figure 2b, shows an acceptable agreement. Pressure distribution and void fraction distribution around the hydrofoil are validated by comparing the predicted numerical results with the experimental results of Sedlář et al. [8] as shown in Figure 3 and Figure 4.



a) Cavitation distribution on the runner blade. [Present study]  
 b) Cavitation distribution on the runner blade. [Balint et al, 2004]  
 Figure 2. Comparison between the cavitation distribution on the blade with Balint et al. results.

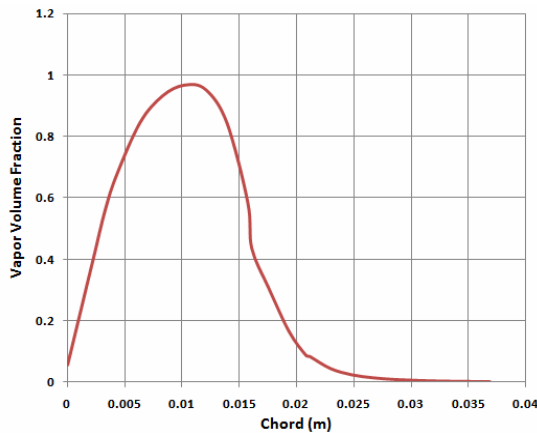


a) Pressure distribution on the hydrofoil after 0.075 Sec. [present study]

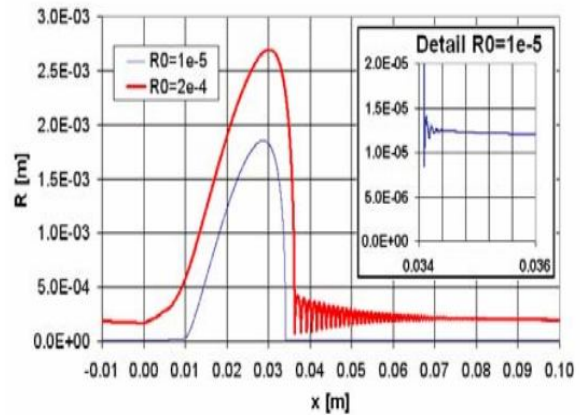


b) Pressure distribution on the hydrofoil [Sedlář et al., 2008].

Figure 3. Comparison between the pressure distributions on the hydrofoil with Sedlář et al. results.



a) Void fraction distribution on the hydrofoil after 0.075 Sec. [Present study].



b) cavitation nucleus on the hydrofoil [Sedlář et al., 2008].

Figure 4. Comparison between void fraction distribution on the hydrofoil with Sedlář et al. results.

## 6. Results and discussion

Figs. 5 and 6 display the void growth computational contours around the rotor and the hydrofoil in a time sequence. After 0.0075 sec the cavity doesn't appear. After 0.022 sec the cavity started to appear at the leading edge on the suction side closer to the hub of the rotor, and the cavity area started to growth and increase in the direction of the tip at the four blades of the axial turbine. After 0.06 sec the cavity formation becomes constant and doesn't vary with time at the four blades of the axial turbine.

Figure 7 shows the density computational contours on the hydrofoil in a time sequence. After 0.0075 sec the density still constant ( $1000 \text{ kg/m}^3$ ) and didn't changed over the blades. After 0.022 sec the density started to decrease only at the leading edge on the suction side closer to the hub of the rotor where the cavity was formed. After 0.06 sec the decreasing in density becomes constant and doesn't vary with time at the four blades of the axial turbine. Figure 8 shows the static pressure computational contours around the hydrofoil in a time sequence. After 0.0075 sec the static

pressure still above the vapor pressure of the water and didn't decreased under the vapor pressure over the blades. After 0.022 sec the static pressure started to decrease less than the vapor pressure only at the leading edge on the suction side closer to the hub of the rotor where the cavity was formed. After 0.06 sec the decreasing in static pressure becomes constant and doesn't vary with time at the four blades of the axial turbine.

Figure 7 shows the density computational contours on the hydrofoil in a time sequence. After 0.0075 sec the density still constant (1000 kg/m<sup>3</sup>) and didn't changed over the blades. After 0.022 sec the density started to decrease only at the leading edge on the suction side closer to the hub of the rotor where the cavity was formed. After 0.06 sec the decreasing in density becomes constant and doesn't vary with time at the four blades of the axial turbine.

Figure 8 shows the static pressure computational contours around the hydrofoil in a time sequence. After 0.0075 sec the static pressure still above the vapor pressure of the water and didn't decreased under the vapor pressure over the blades. After 0.022 sec the static pressure started to decrease less than the vapor pressure only at the leading edge on the suction side closer to the hub of the rotor where the cavity was formed. After 0.06 sec the decreasing in static pressure becomes constant and doesn't vary with time at the four blades of the axial turbine.

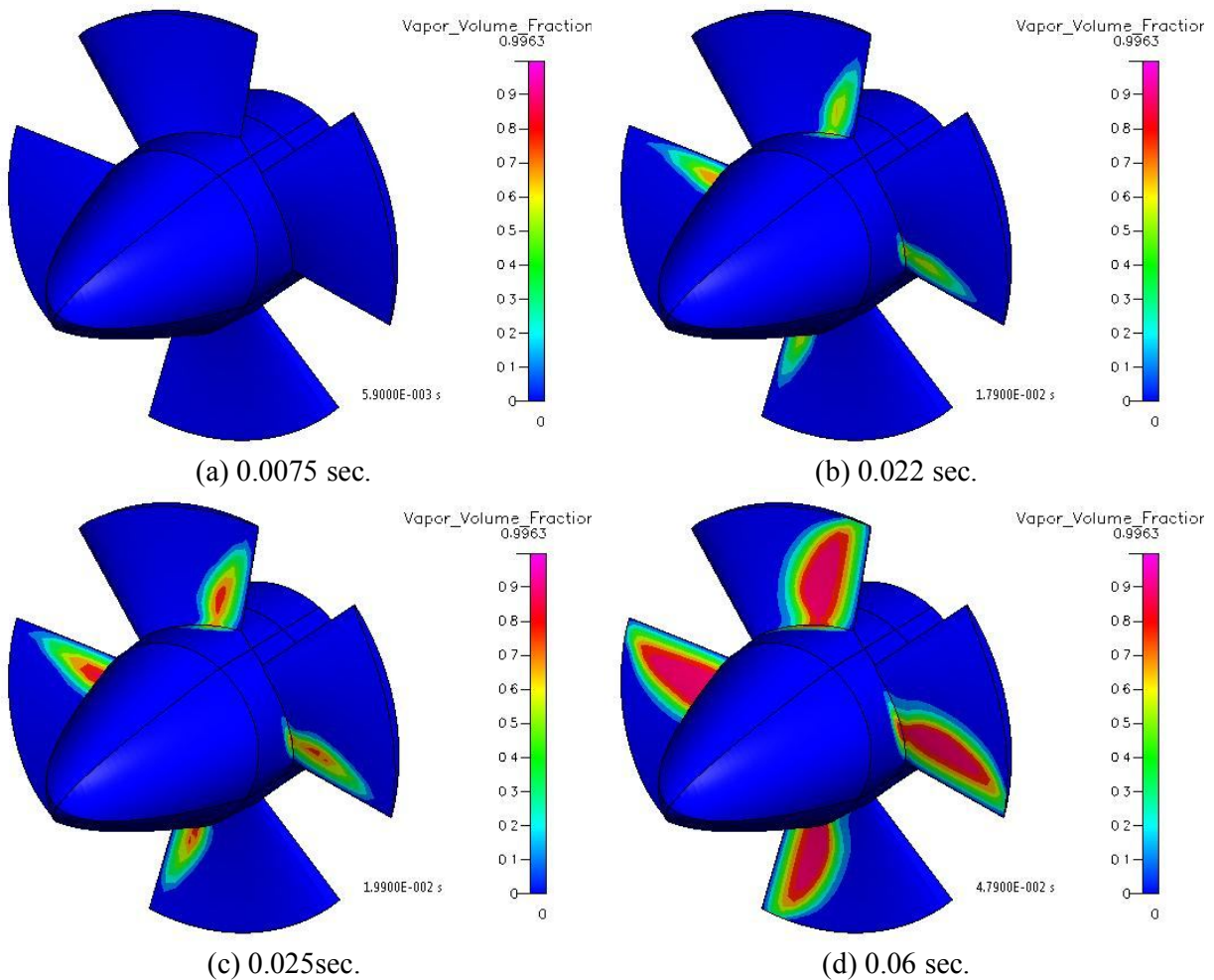


Figure 5. Vapor volume fraction contours around the rotor, 2000 rpm,  $\beta_1 = 80^\circ$  and  $\beta_2 = 80^\circ$ .

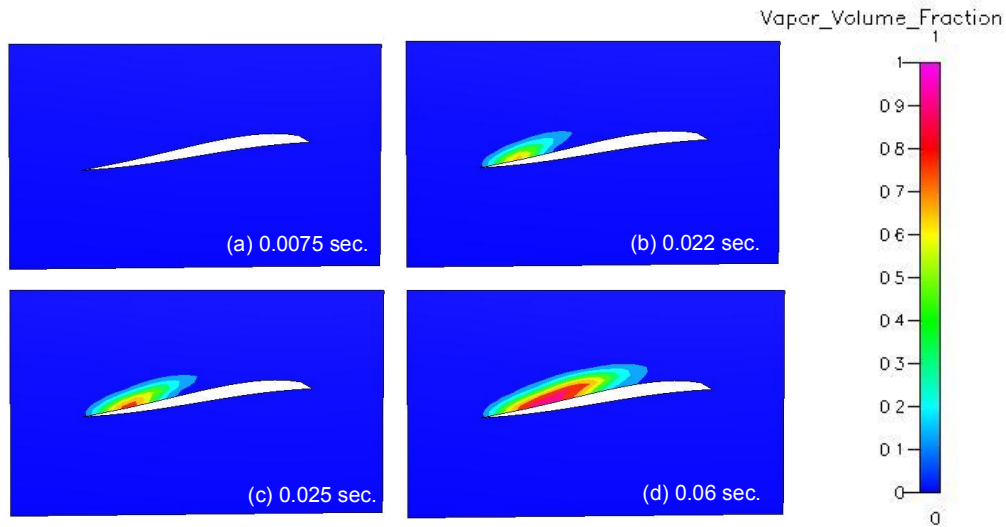


Figure 6. Vapor volume fraction contours at the mid-section of the hydrofoil, 2000 rpm,  $\beta_1 = 80^\circ$  and  $\beta_2 = 80^\circ$ .

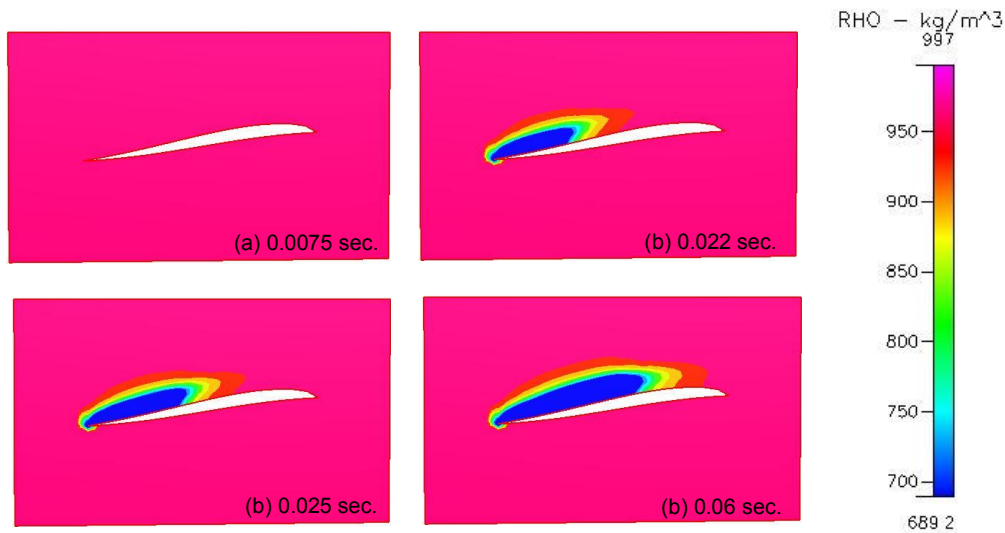


Figure 7. Density contours at the mid-section of the hydrofoil, 2000 rpm,  $\beta_1 = 80^\circ$  and  $\beta_2 = 80^\circ$ .

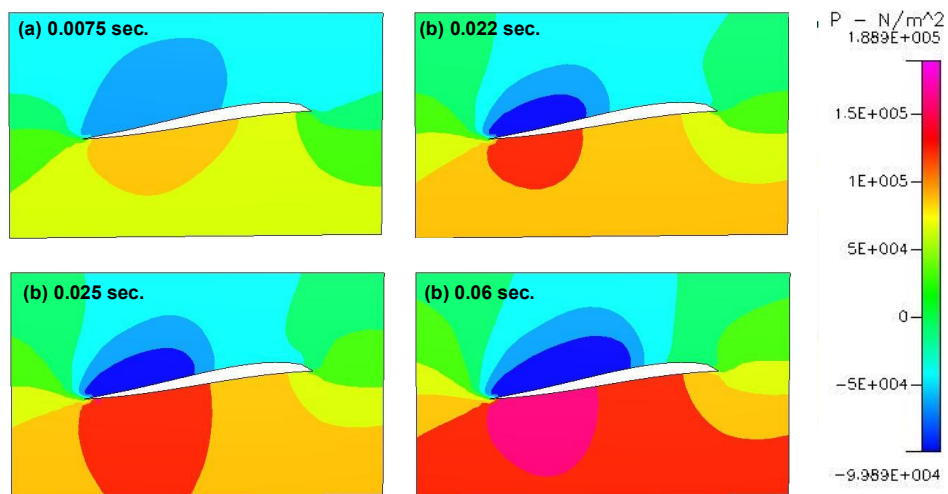
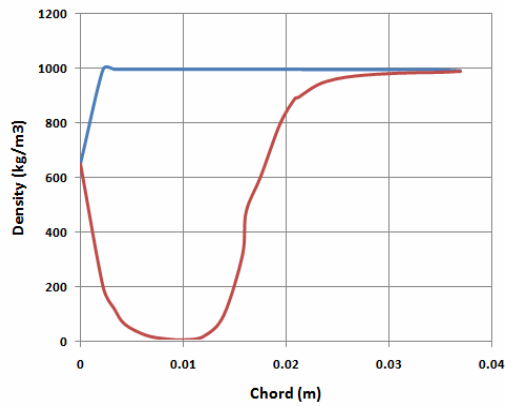


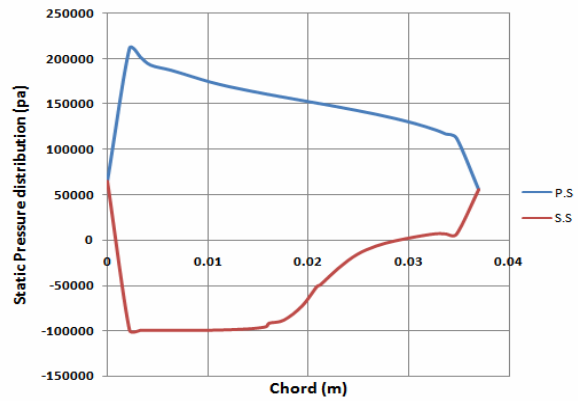
Figure 8. Static pressure contours at the mid-section of the hydrofoil, 2000 rpm,  $\beta_1 = 80^\circ$  and  $\beta_2 = 80^\circ$ .

$$\beta_2 = 80^\circ.$$

Fig. 9 shows the density, static pressure, total pressure and vapor volume distribution respectively on the hydrofoil at the mid section. The density decreases at the leading edge of the suction side of the hydrofoil, then it increases at the trailing edge of the hydrofoil. The static pressure decreases at the leading edge of the suction side of the hydrofoil, then it increases at the trailing edge of the hydrofoil. It is obvious that the pressure decreases sharply at the leading edge at the tip section where the cavity is appeared. The void fraction increases at the leading edge of the suction side of the hydrofoil, then it decreases at the trailing edge of the hydrofoil. It is obvious that the void fraction increases sharply at the leading edge.

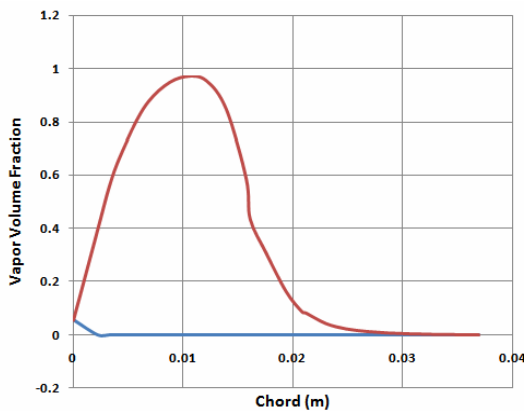


(a) Density distribution on the hydrofoil

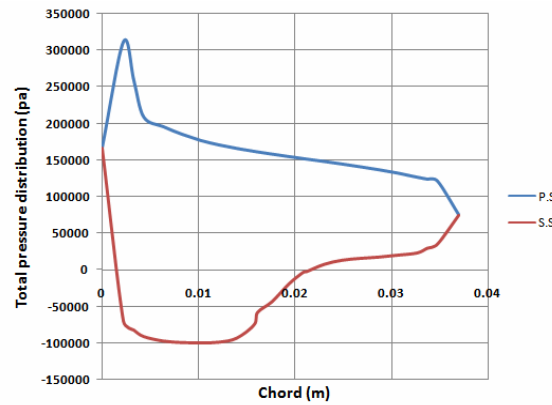


(b) Static Pressure distribution on the hydrofoil

**Fig. 9a** Density, Static pressure, Total pressure and void fraction distribution at the Mid-section of the hydrofoil after 0.075 sec, 2000 rpm,  $\beta_1 = 80^\circ$  and  $\beta_2 = 80^\circ$ .



(c) Vapor volume fraction distribution on the hydrofoil



(d) Total pressure on the hydrofoil

**Fig. 9b** Density, Static pressure, Total pressure and void fraction distribution at the Mid-section of the hydrofoil after 0.075 sec, 2000 rpm,  $\beta_1 = 80^\circ$  and  $\beta_2 = 80^\circ$ .

## 7. Summary and conclusions

A numerical study was performed to simulate the cavitation phenomenon in axial turbine. The numerical simulation was done using a commercial CFD code called CFD-ACE which uses the "The full cavitation model" to predict the cavitation in axial turbine. From the results of the present study, the following conclusions are drawn:

- 1- The cavitation inception was caught on the suction side of the runner blade
- 2- The computational code has been validated by comparing the predicated numerical results with the previous studies. The comparison shows good agreement.
- 3- In axial turbine cavitation occurred at blade angle  $80^\circ$  and not appeared at blade angles  $60^\circ$  and  $70^\circ$ , as an important result, just by adjusting the blade angle to  $60^\circ$  or  $70^\circ$ , cavitation can be avoided.
- 4- Corresponding to the pressure distribution, the highest cavity void fraction area appears where the pressure is lowest on the suction side of blade.
- 5- Because the pressure on the pressure side is higher than the saturated vapor pressure of water, there is not any cavitation.
- 6- In axial turbine the cavity formation has mainly three stages. First, a cavity starts to grow at the leading edge of all blades of the impeller after 0.022 sec only due to its low pressure. The second stage, the cavity grows over the blades of the axial turbine after 0.025 sec. Finally, after 0.06 sec that cavity starts to fluctuate at the leading edge of the rotor and the cavitated area becomes constant and doesn't change with time.

## Nomenclature

### Roman

$C_e, C_c$	Phase change rate coefficients	
$C_N$	Slip speed factor "ratio between rotor actual rotational speed and theoretical rotating frame speed"	
$f$	Vapor mass fraction	
$k$	Turbulence kinetic energy	$m^2/s^2$
N	Turbine rotational speed	r.p.m.
P	Fluid static pressure	$N/m^2$
$p_{sat}$	Saturation pressure	$N/m^2$
$P'_{turb}$	The magnitude of pressure fluctuations	$N/m^2$
$P_t$	Total pressure	$N/m^2$
$P_v$	Vapor pressure	$N/m^2$
R	Universal gas constant	$Nm/mol.k$
$R$	Phase change rate	
$Re_n$	Reynolds number	
T	Fluid temperature	K
$\Delta t$	Physical time step	second
$\vec{V}$	Velocity vector	
$V_{ch}$	Characteristic velocity $V_{ch} = \sqrt{k}$	
W	Molecular weight	$kg/kg\text{-mol}$

### Greek

$\beta_1$	Blade inlet angle (angle between the tangent to camber line at inlet and the axial direction)	degree
$\beta_2$	Blade outlet angle (angle between the tangent to camber line at outlet and the axial direction)	degree
$\alpha_v$	Vapor volume fraction	
$\alpha_g$	gas volume fraction	
$\sigma$	Cavitation number $((p_\infty - p_v) / (1/2 \rho_l u^2))$	--
$\rho$	The mixture density	$Kg/m^3$
$\Gamma$	Effective exchange coefficient	

### Suffixes

$c$	Bubble reduction and collapse	$L$	Liquid phase
-----	-------------------------------	-----	--------------

$e$	Bubble generation and expansion	$V$	Vapor phases
$Gas, G$	Gaseous phase		

## References

- [1] Mostafa, N. H., Rayan, M. A., and Mahgob, M. M. *Energetic model for cavitation erosion prediction in centrifugal pump impeller*. In *1990 Proceeding of ASME/CSME Cavitation and Multiphase flow forum*, Toronto, Canada. PP 133-138.
- [2] Nilsson, H., and Davidson, L. *A numerical investigation of tip clearance flow in Kaplan water turbines*. In *1990 proceedings of Hydropower into the next century*. Vol. III.
- [3] Grekula, M., and Bark, G. *Experimental Study of Cavitation in a Kaplan Model Turbine*. CAV2001, session B9.004.
- [4] Balint, D., Resiga, R., Muntean, S., Ruprecht, A., and Goede, E. *High performance computing of self induced unsteadiness cavitating flows in hydro turbine*. Romania, National Center for Engineering of Systems with Complex Fluids, 2004.
- [5] Escaler, X., Egusquiza, E., Farahat, M., Avellan, F., and Coussirat, M. *Detection of cavitation in hydraulic turbines*. Mechanical Systems and Signal Processing, 2006. 20, pp 983-1007.
- [6] Mostafa, N. H. and Boraey, M. A. *Numerical and Experimental Investigation of Cavitation in Axial Pumps*. In *2006 8<sup>th</sup> International Congress of Fluid Dynamics and Propulsion*, Sharm El-Sheikh, Sinai, Egypt, Dec. 14-17.
- [7] Liu, S., Chen, Q., and Wu, Y. *Unsteady Cavitating Turbulent Flow Simulation In A Kaplan Turbine*. In *2007 Proceedings of the 2nd IAHR International Meeting of the Workgroup on Cavitation and Dynamic Problems in Hydraulic Machinery and Systems*.
- [8] Sedlář, M., Zima, P., Němec, T., and Maršík, F. *Analysis of Cavitation Phenomena in Water and its Application to Prediction of Cavitation Erosion in Hydraulic Machinery*. In *2008 ICPWS XV*, Berlin.
- [9] Singh, P., and Nestmann, F. *Experimental optimization of a free vortex propeller runner for micro hydro application*. Experimental Thermal and Fluid Science, 2009. 33, pp 991–1002.
- [10] CFD-ACE V2008 Modules Manual – Volume 1, May 1, 2008.
- [11] CFD-ACE V2008 User Manual – Volume 1, May 1, 2008.
- [12] Hinze, J.O., *Turbulence*. McGraw-Hill Book Co., Second Edition, 1975.
- [13] Hammitt, F. G. *Cavitation and multiphase flow phenomena*. McGraw-Hill-Book Co., 1980.
- [14] Pereira, F., Salvatore, F. and Felice F. *Measurement and Modeling of propeller cavitation in uniform inflow*. Transactions of the ASME, Journal of Fluid Engineering, 2004. 126, pp. 671-679.
- [15] Fukaya, M., Okamura, T., Tamura, Y., Matsumoto, Y. *Prediction of Cavitation Performance of Axial Flow Pump by Using Numerical Cavitating Flow Simulation with Bubble Flow Model*. Fifth International Symposium on Cavitation, 2003, Osaka, Japan. November 1-4.